Internal and external magnetic-field engineering of negative magnetization and exchange bias in $La_{1-x}Pr_xCrO_3$ ($0.8 \leqslant x \leqslant 0.9$)

Deepak Garg [1,2,3,4,*] Amit Kumar [1,3,†] S. M. Yusuf,[1,3,‡] Markos Skoulatos,[5] Sachindra Nath Sarangi [2] Dinesh Topwal [2,3] and Yixi Su [4]

[1]*Solid State Physics Division, Bhabha Atomic Research Centre, Mumbai 400085, India*

[2]*Institute of Physics, Sachivalaya Marg, Bhubaneswar 751005, India*

[3]*Homi Bhabha National Institute, Anushaktinagar, Mumbai 400094, India*

[4]*Jülich Centre for Neutron Science (JCNS) at Heinz Maier-Leibnitz Zentrum (MLZ), Forschungszentrum Jülich GmbH, Lichtenbergstr.1, Garching D-85748, Germany*

[5]*Heinz Maier-Leibnitz Zentrum (MLZ) and Physics Department, Technical University of Munich, Garching D-85748, Germany*

(Received 18 January 2025; revised 23 April 2025; accepted 29 April 2025; published 19 May 2025)

The negative magnetization and exchange bias phenomena have been the subject of interest due to their promising applications in spintronic devices. In this study, we have comprehensively investigated these two intertwined magnetic phenomena in $La_{1-x}Pr_xCrO_3$ ($x = 0.8-0.9$) compounds. The Cooke's model fit to dc magnetization data infers negative internal magnetic field for $x = 0.8$, 0.85, and 0.87 and positive for $x = 0.9$. The crossover of internal magnetic field from negative to positive across $x = 0.87$ and its dominance over the external applied magnetic field leads to the magnetization switching from negative to positive. The internal magnetic field behavior also explains the anomalous magnetization behavior involving reduced magnetization for $x = 0.87$, despite having higher Pr^{3+} concentration than that for $x = 0.8$ and 0.85. The anomalous magnetization is corroborated well by the neutron depolarization experiments, where no depolarization is observed for $x = 0.87$ owing to nearly compensated domain magnetization. Remarkably, a switching of the exchange bias from inverse (with positive H_{EB}) to conventional (with negative H_{EB}) due to a competition of external and internal magnetic fields is found in $x = 0.8$ and 0.85 compounds. The $x = 0.87$ and 0.9 compounds, on the other hand, show only conventional exchange bias at all measured magnetic fields. Using the Cooke's model, we show that the antiferromagnetic coupling between polarized Pr^{3+} and weak ferromagnetic component of canted Cr^{3+} moments explain not only the inverse exchange bias but the conventional exchange bias as well, however, the moment orientations are different for both types of exchange bias. Moreover, our study demonstrates that the ferromagnetic coupling between the two moments can also lead to conventional exchange bias, similar to that observed in interfacial heterostructure systems.

DOI: 10.1103/PhysRevMaterials.9.054406

I. INTRODUCTION

In the recent years, the study of exchange bias (EB) and unusual negative magnetization (NM) phenomena has gained intense research interest due to their significance in fundamental physics as well as potential technological importance in thermomagnetic switches [1], spin valves [2], high-density magnetic storage [3], voltage-mediated magnetic switching [4], and various spintronic devices [5]. In the NM phenomenon, the order parameter, magnetization (M) changes its sign from positive to negative during decrease of temperature under some external magnetic field (H) and the temperature at which magnetization becomes zero is called compensation temperature (T_{COMP}) [1]. The EB, on the other side, is manifested by shifting of the hysteresis loop and is characterized by the exchange bias shift parameters H_{EB} (and M_{EB}). Following its discovery in Co/CoO core-shell nanoparticles by Meiklejohn and Bean [6], EB was mainly studied in core-shell nanoparticles [7–9] and in various magnetic heterostructures involving different phases like ferromagnetic (FM), antiferromagnetic (AFM), and spin glass [10,11]. In most of these systems, only conventional EB with negative H_{EB} was reported [7–11], however, inverse EB with positive H_{EB} was reported in few systems only [12,13]. The AFM and FM exchange coupling at the interface between two magnetic phases causes a pinning effect and this was understood to be a cause of positive and negative H_{EB}, respectively [13,14]. From the last two decades, research of EB is extended to homogeneous magnetic compounds (without any real interface), where similar to interfacial systems, conventional EB was reported [15–17]. However, the origin of EB in these systems is found to be different and is related to the intrinsic exchange coupling between magnetic sublattices present.

*Contact author: deepak1.phy@gmail.com
†Contact author: amitkr@barc.gov.in
‡Contact author: smyusuf@barc.gov.in

Recently, attention has been given to study EB in magnetic compounds showing the NM phenomenon [18,19]. Interestingly, in these compounds, similar to NM, EB also shows sign reversal across the T_{COMP} leading to both inverse and conventional EB below and above the T_{COMP}, respectively [20–23]. Such concurrent occurrences of inverse and conventional EB are quite appealing, rendering these compounds further useful for thermal-assisted magnetic random access memory devices [24]. Literature studies show that NM-based perovskite compounds, particularly RBO_3 [with magnetic R (rare earth) and B = Cr, Fe], show such a remarkable H_{EB} reversal with temperature [20,21,23,25]. However, the sign reversal of H_{EB} with magnetic field in these compounds is seldom observed [26]. Among various studied RBO_3 compounds, $La_{1-x}Pr_xCrO_3$ are found particularly interesting. Our recent study on $La_{1-x}Pr_xCrO_3$ (x = 0, 0.25, 0.5, 0.75, and 1) [27,28] compounds show a correlation among NM, EB, and electrical properties. The study also demonstrated the sign reversal of H_{EB} from positive to negative across $x = 0.75$. The T_{COMP} was found to increase with increasing x, became maximum for the $x = 0.75$ followed by a decrease [28]. The electrical conduction mechanism also changed across $x = 0.75$. In these compounds, it is also reported that the NM phenomenon disappears at $x > 0.85$ [29,30]. However, the physics behind the mysterious disappearance of NM in these compounds is not known so far. Further, Yoshi *et al.* [30] reported positive and negative H_{EB} in $La_{1-x}Pr_xCrO_3$ (x = 0.75 and 0.85) compounds under the conditions of cooling magnetic field (H_{COOL}) < internal magnetic field (H_I) and $H_{COOL} > H_I$, respectively. They explained the positive and negative H_{EB} based on the AFM and FM coupling between Pr^{3+} and weak ferromagnetic Cr^{3+} moments, respectively, as explained in the literature for the heterostructure systems [13,14]. However, an in-depth or detailed explanation of the experimental EB results was not provided. Therefore, to shed light on the unusual NM disappearance and EB behavior with H_{COOL}, in this study, we have investigated $La_{1-x}Pr_xCrO_3$ ($x = 0.8$ to 0.9) compounds using comprehensive dc magnetization, neutron diffraction, and neutron depolarization studies.

Our dc magnetization data analysis using the Cooke's model reveals that the polarized Pr^{3+} (M_{Pr}) and FM component of canted Cr^{3+} (M_{Cr}) moments are coupled in various configurations like M_{Cr} up (↑), M_{Pr} down (↓); M_{Cr} down (↓), M_{Pr} up (↑); M_{Cr} up (↑), M_{Pr} down (↑) depending upon the applied magnetic field. These M_{Cr} and M_{Pr} spin orientations not only explain the NM and its disappearance but also explain the anomalous magnetization behavior in these compounds involving decreasing magnetization upto $x = 0.87$ followed by an increase. Interestingly, the changing orientation of M_{Pr} and M_{Cr} moments with magnetic field also explains the inverse ($x = 0.8$ and 0.85) and conventional (x = 0.8, 0.85, 0.87, and 0.9) EB in these compounds. This study also reveals that NM and EB have the same underlying physics origin and these two magnetic phenomena are indeed intertwined with each other.

II. EXPERIMENTAL DETAILS

The polycrystalline powder samples of $La_{1-x}Pr_xCrO_3$ were prepared by the solid-state reaction method, as described in Refs. [27,28]. The single phase of the samples was confirmed using a laboratory source-based x-ray diffraction data recorded at room temperature (see Sec. S1 in the Supplemental Material (SM) [31]). The dc magnetization $M(T)$ measurements were carried out on all powder samples in the temperature range of 5–300 K under various magnetic fields in field-cooled-cooling (FCC) and field-cooling-warming (FCW) modes. In the FCC mode, the dc magnetization was measured while cooling the sample under a magnetic field, while in the FCW mode, the dc magnetization was measured in the warming cycle under the same magnetic field applied for the FCC measurement. For EB measurements, the $M(H)$ hysteresis loops were recorded at various temperatures by sweeping the magnetic field over ±50 kOe in field-cooled (FC) mode. In field-cooled (FC) hysteresis loop measurements, each sample was cooled from room temperature down to a measuring temperature under a given magnetic field, and then hysteresis loop was recorded. After every hysteresis loop measurement, the sample was heated to room temperature (above the magnetic ordering temperature) for demagnetization. For both types of the dc magnetization measurements, the Physical Property Measurement System (PPMS) DynaCool 14 of the Physics Lab at the Heinz Maier-Leibnitz Zentrum (MLZ) and the SQUID magnetometer at the Institute of Physics (IOP) were used. The neutron depolarization experiments using polarized neutrons were carried out on all powder samples in the temperature range of 5–300 K under a magnetic field of 50 Oe using the Polarized Neutron Spectrometer ($\lambda = 1.201$ Å) at Dhruva reactor, Bhabha Atomic Research Centre (BARC), Mumbai, India. The neutron powder diffraction experiments over the temperature range of 5 to 300 K under zero magnetic field were carried out using the position-sensitive detector-based powder diffractometer-I ($\lambda = 1.094$ Å) at Dhruva reactor, BARC, Mumbai, India. The x-ray and neutron diffraction data were analyzed by the Rietveld refinement technique [32] using FULLPROF software package [33].

III. RESULTS

A. dc magnetization

Figure 1 shows the temperature-dependent dc magnetization of $La_{1-x}Pr_xCrO_3$ ($x = 0.8$, 0.85, 0.87, and 0.9) compounds in $H = 100$ Oe recorded in field-cooled-cooling (FCC) mode. The $x = 0.8$, 0.85, and 0.87 compounds show the interesting phenomenon of NM with the compensation temperatures (T_{COMP}) of 216, 222, and 198 K, respectively [Figs. 1(a)–1(c)]. The NM phenomenon disappears for $x >$ 0.87 and thus the $x = 0.9$ compound shows only positive M in the entire magnetic ordering state (below T_N) [Fig. 1(d)]. The magnetization behaviors align well with the literature findings [29,30]. The magnetic ordering temperature (T_N) is found to be decreasing from 250 K for $x = 0.8$ to 242 K for $x = 0.9$, which is also consistent with the decreasing trend of T_N with increasing x in $La_{1-x}Pr_xCrO_3$ compounds [28,34]. Further, the M data under $H = 100$ Oe as a function of x at some selected temperatures are plotted in Fig. 1(e). The M values for x = 0.25, 0.5, 0.75, and 1 compounds, taken from our previous study [28], are also plotted in Fig. 1(e) to see complete x dependence of M in $La_{1-x}Pr_xCrO_3$ series.

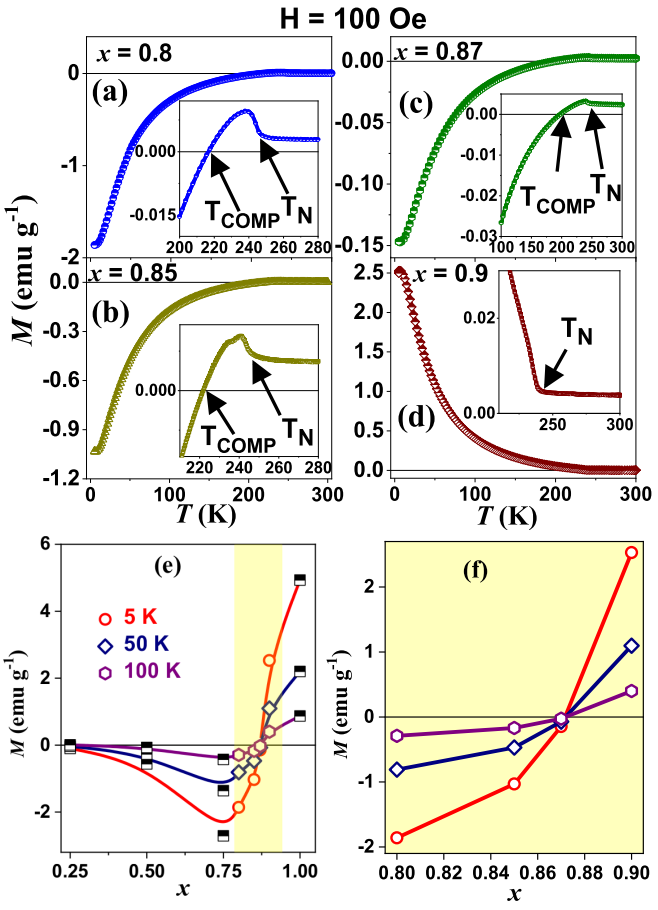

FIG. 1. (a)–(d) The dc magnetzation (M) vs temperature (T) curves of $La_{1-x}Pr_xCrO_3$ ($x = 0.8$, 0.85, 0.87, and 0.9) compounds recorded in field-cooled-cooling (FCC) mode under $H = 100$ Oe. Insets show the zoomed view of M near the transition temperatures (T_{COMP} and T_N). (e) The x dependence of M at some selected temperatures. The half-filled black squared symbol data are taken from Ref. [28]. (f) Enlarged view of highlighted yellow region of M vs x curves in (e).

As shown in Fig. 1(e), the $x = 0.75$ compound exhibits the higher negative M than that for all other NM compounds of this series. It is also evident that with increasing x from 0.75, negative M value at a given T starts to decrease, changes sign from negative to positive across $x = 0.87$ with minimum negative M, and then remains positive with increasing M, thus indicating an anomalous M behavior [Figs. 1(e) and 1(f)] in the compounds of $La_{1-x}Pr_xCrO_3$ series. Here it should be noted that the initial increase in M up to $x = 0.75$ is consistent with the increasing Pr^{3+} concentration in $La_{1-x}Pr_xCrO_3$ as Pr^{3+} is a magnetic ion with an effective magnetic moment of $\sim 3.58\,\mu_B$. However, a decrease in M for $x > 0.75$ and the lowest M observed for $x = 0.87$ are totally unusual as these compounds have higher magnetic Pr^{3+} concentration than that of $x \leqslant 0.75$. This nonmonotonic M behavior should be related with the different orientations of Pr^{3+} and Cr^{3+} moments with changing x. The mesoscopic and domain-level understanding of the anomalous M behavior has been obtained by neutron depolarization experiments performed using polarized neutrons (see next section). Moreover, we have fitted the dc magnetization data using the Cooke's model to get an insight into the anomalous M behavior in these compounds (see Discussion section).

To get a detailed understanding of the NM in $x = 0.8$, 0.85, and 0.87 compounds, the M vs T data have been recorded under various magnetic fields and the results are displayed in Figs. 2(a)–2(c). The $x = 0.8$ compound shows the NM phenomenon up to a magnetic field of 5 kOe [Fig. 2(a)]. Interestingly, for $H = 5$ kOe, a sharp upturn at low temperature is observed in the M vs T curve, leading to a further change in M sign from negative to positive, i.e., two T_{COMP} for the compound. A similar sharp upturn is also observed for $H > 5$ kOe M vs T curves, however, M remains positive throughout the measured temperature range. The $x = 0.85$ compound shows the M behavior under various H similar to the $x = 0.8$, except that the H is decreased from 5 to 2 kOe to observe the NM phenomenon [Fig. 2(b)]. In contrast to $x = 0.8$ and 0.85, the NM phenomenon disappears at a relatively small H (> 200 Oe) for $x = 0.87$ [Fig. 2(c)]. The variation of T_{COMP} with H for $x = 0.8$ and 0.85 compounds is shown in Fig. 2(d). The T_{COMP} is found to be decreasing with increasing H. The T_{COMP} also decreases with increasing x. The $x = 0.9$ shows only positive magnetization at all applied H, for instance, see M vs T curves under $H = 1$ and 5 kOe [Fig. S2 in SM [31]]. Similar to M behavior, interesting EB results (presented later) are also found for these compounds. In the EB section; we see that $x = 0.8$ and 0.85 compounds show inverse and conventional EB, i.e., sign reversal of H_{EB} from positive to negative with variation of cooling magnetic field (H_{COOL}). While the $x = 0.87$ and 0.9 compounds show only conventional EB for all measured H_{COOL}.

B. Neutron depolarization

To understand the anomalous M behavior of $La_{1-x}Pr_xCrO_3$ compounds at the mesoscopic or domain-level length scales, the one-dimensional (z-z) neutron depolarization experiments are carried out over the temperature range of 5–300 K under $H = 50$ Oe. In these experiments, polarized neutrons (with polarization ~98.8% along the z direction) are incident on the sample under study, and final neutron beam polarization (P_f) is measured. It should be noted that paramagnets, collinear antiferromagnets, and canonical spin-glass systems, having average zero magnetization at the mesoscopic length scales, do not cause any depolarization of the polarized neutron beam. The other details of the instrument are given elsewhere [35,36]. The P_f for $La_{1-x}Pr_xCrO_3$ ($x = 0.8$, 0.85, 0.87, and 0.9) compounds as a function of the temperature (5–300 K) is shown in Fig. 3(a). It is evident that P_f shows a monotonic decrease right below ~ 120 and 100 K for $x = 0.8/0.9$ and 0.85 compounds, respectively, indicating an increase in domain magnetization with decreasing temperature. On the other hand, no neutron beam depolarization for $x = 0.87$ in the whole measured temperature range represents the almost compensated magnetic state with nearly zero-domain magnetization. The P_f as a function of x at 5 and 50 K are plotted in Fig. 3(b). Interestingly, the P_f data reflect the M behavior shown in Fig. 1(f), thus providing a mesoscopic understanding of the anomalous M behavior over the magnetic domain length scale.

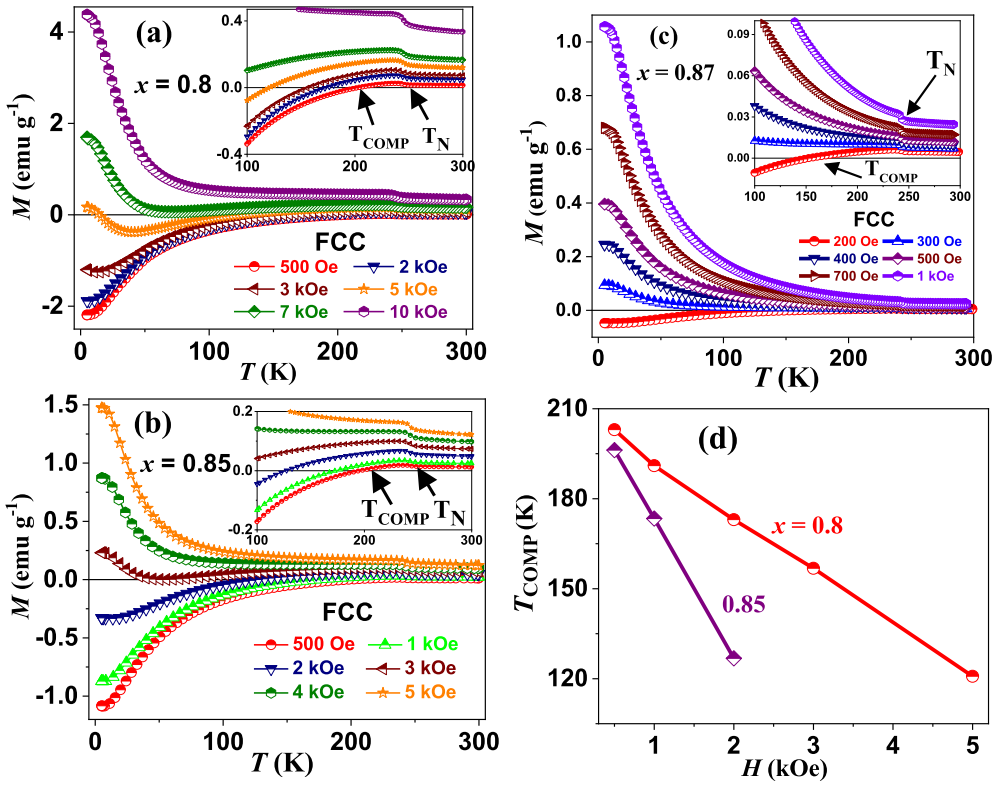

FIG. 2. FCC M vs T curves for (a) $x = 0.8$, (b) $x = 0.85$, and (c) 0.87 recorded under various H. Insets show the zoomed view of M vs T curves near the T_{COMP} and T_N. (d) Variation of T_{COMP} with H.

Since $La_{1-x}Pr_xCrO_3$ ($x = 0.8$, 0.85, and 0.9) compounds show finite depolarization of incident polarized neutron beam, therefore we have estimated the average domain size of these compounds using the following equation [35,36]:

$$P_f = P_i \exp\left[-\alpha\left(\frac{d}{\delta}\right)\langle\Phi_\delta\rangle^2\right], \tag{1}$$

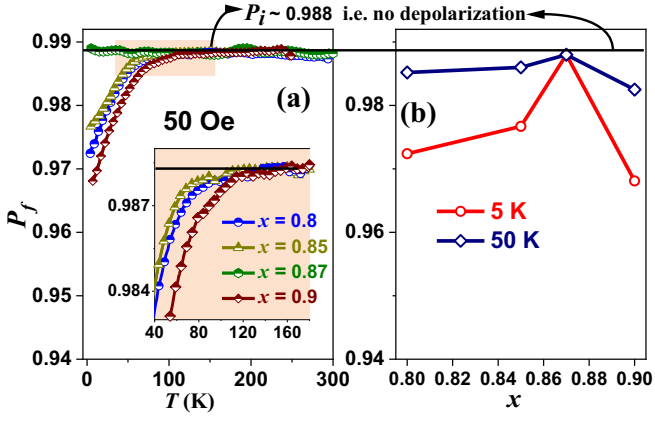

FIG. 3. (a) The transmitted neutron beam polarization (P_f) vs temperature (T) curves for $La_{1-x}Pr_xCrO_3$ ($x = 0.8$, 0.85, 0.87, and 0.9) compounds recorded under $H = 50$ Oe. The zoomed-view of highlighted P_f curves is shown in the inset displaying the onset of neutron depolarization below ~100 and ~120 K for $x = 0.85$ and 0.8/0.9, respectively. (b) The x dependence of P_f for $x = 0.8$ to 0.9 at 5 and 50 K. The black line in both figures at $P_f \sim 0.988$ indicates the zero neutron depolarization line.

where P_i/P_f is the initial/final neutron beam polarization, α (~1/3) is a dimensionless parameter, d (~4.4 mm) is the effective thickness of the samples, and $\Phi_\delta = (4.63 \times 10^{-10}\ \mathrm{G^{-1}\,\AA^{-2}})\lambda B\delta$ is the precession angle for a neutron of wavelength λ (= 1.201 Å) traveling a distance δ (average domain size) inside a domain of magnetization B ($= 4\pi M_s\rho$). Here, M_s and ρ are the saturation magnetization and density of the compounds in emu g^{-1} and g cm^{-3}, respectively. Using all these parameters in Eq. (1), $\delta \sim 2(1)$, 1.54(10), and 4(2) μm at 5 K for $x = 0.8$, 0.85, and 0.9 compounds, respectively, are estimated. Thus, the $x = 0.8$, 0.85, and 0.9 compounds have almost same average domain size, at least within the certainty of our experimental resolution. It may be noted from Eq. (1) that neutron depolarization depends on the product of domain magnetization and domain size. Since the compounds have almost same average domain size, therefore, the depolarization is mainly governed by the domain magnetization in the samples.

C. Exchange bias

To study the EB in $La_{1-x}Pr_xCrO_3$ ($x = 0.8$, 0.85, 0.87, and 0.9) compounds, the hysteresis loops are recorded at various temperatures by cooling the compounds under 5 kOe magnetic field (H_{COOL}). Figure 4(a) shows the hysteresis loops for all four compounds at 100 K. It is worth noting that for $x = 0.8$ and 0.85, the hysteresis loops shift towards the positive magnetic field axis, i.e., along $+H$ with $+H_{COOL}$, indicating the presence of inverse EB. While the hysteresis loops are found to be shifted along the negative magnetic

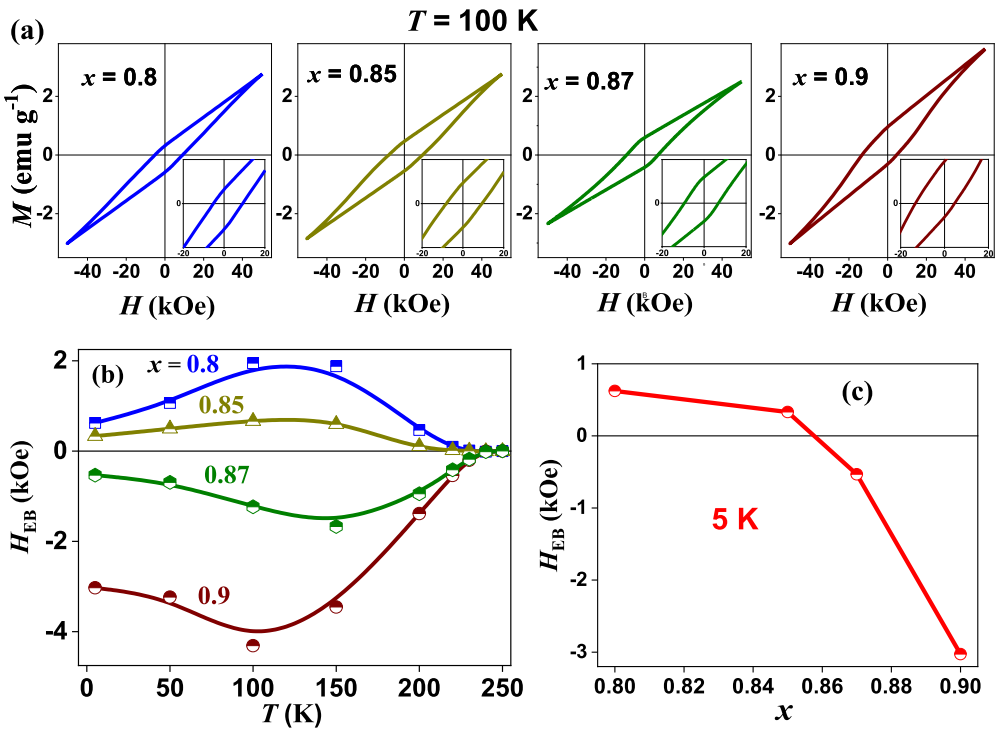

FIG. 4. (a) Field-cooled (H_{COOL} = 5 kOe) hysteresis loops of $La_{1-x}Pr_xCrO_3$ (x = 0.8, 0.85, 0.87, and 0.9) compounds at 100 K. Zoomed view of the hysteresis loops is shown in the inset for better clarity of EB. (b) Temperature dependence of H_{EB} for all compounds. (c) Variation of H_{EB} with x at 5 K.

field axis, i.e., along $-H$ with $+H_{COOL}$, for $x = 0.87$ and 0.9, thus revealing conventional EB in these compounds. The EB field is defined as $H_{EB} = \frac{H_{C1} + H_{C2}}{2}$, here H_{C1} and H_{C2} are the coercive fields for the descending and ascending branches of $M(H)$ hysteresis loop, respectively. The temperature dependence of H_{EB} is shown in Fig. 4(b). Interestingly, the NM compounds, i.e., x= 0.8 and 0.85 exhibit inverse EB with apparent positive $H_{EB} > 50$–100 Oe at all the temperatures below 220 K ($\sim T_{COMP}$) and 200 K ($< T_{COMP}$), respectively, while above these temperatures, a very small $H_{EB} \sim -20$ Oe is observed. The positive H_{EB} is consistent with the literature reports on other Cr-based NM compounds [23,37–39] as well as matches with our previous studies on $YbCrO_3$ [20] and $La_{1-x}Pr_xCrO_3$ ($0.25 \leqslant x \leqslant 0.75$) [27,28]. The non-NM compound (i.e., x= 0.9), on the other hand, exhibits usual negative H_{EB} throughout the $T < T_N$ range, which is also consistent with the literature on other non-NM compounds [17,40]. However, for the critical composition, $x = 0.87$ of $La_{1-x}Pr_xCrO_3$, the negative H_{EB} is found, which is indeed a fascinating observation. The remanence asymmetry (M_{EB}) is also calculated using the expression $M_{EB} = \frac{M_{R1} + M_{R2}}{2}$, where M_{R1} and M_{R2} are the upper and lower remanent magnetizations of $M(H)$ hysteresis loop, respectively. The M_{EB} exhibits the similar temperature dependence as that of H_{EB} except with the opposite sign, i.e., negative for $x = 0.8$, 0.85 and positive for $x = 0.87$, 0.9 compounds [Fig. S3(a) in SM [31]].

The H_{EB} as a function of x at 5 K is plotted in Fig. 4(c). It should be noted that similar to M behavior [Fig. 1(f)], H_{EB} is also changing its sign, however, from positive to negative across $x = 0.87$, indicating that both NM and EB are correlated with each other and have the same underlying origin. Interestingly, H_{EB} vs x [Fig. 4(c)] variation is found similar to the M_{Cr} (FM Cr^{3+} moment) and H_I (internal field) vs x [see highlighted part of Figs. 7(b) and 7(c)], calculated from the Cooke's model fit (see Discussion section), demonstrating the role of orientations of coupled M_{Cr} and polarized Pr^{3+} (M_{Pr}) moments in the sign reversal of H_{EB} in the present series of $La_{1-x}Pr_xCrO_3$ compounds.

To understand the EB results for $x = 0.8$, 0.85, and 0.87 under $H_{COOL} = 5$ kOe, we have further performed detailed EB experiments under various H_{COOL}. The calculated H_{EB} for these compounds are plotted in Fig. 5. Interestingly, both $x = 0.8$ and 0.85 compounds show the sign reversal of H_{EB} from positive to negative across ~18 kOe and ~7 kOe, respectively [Figs. 5(a)–5(d)]. It is interesting to note that these values are close to their corresponding maximum $|H_I|$ values, calculated from the Cooke's model fit (see Discussion section). On the other hand, the $x = 0.87$ compound shows negative H_{EB} [Fig. 5(e)] at all H_{COOL}s. The M_{EB} is also calculated for these compounds and results are plotted in Figs. S3(b)–S3(d) in SM [31]. Similar to H_{EB}, the sign reversal of M_{EB}, however, with opposite polarity, is observed with H_{COOL} for $x = 0.8$ and 0.85 compounds, while the $x = 0.87$ shows only positive M_{EB}. Thus, our comprehensive investigation indicates that EB in these NM compounds can be tuned using both external and internal magnetic fields. In the Discussion section, we show how the coupled M_{Cr} and M_{Pr} moments with different orientations lead to the striking EB in these compounds.

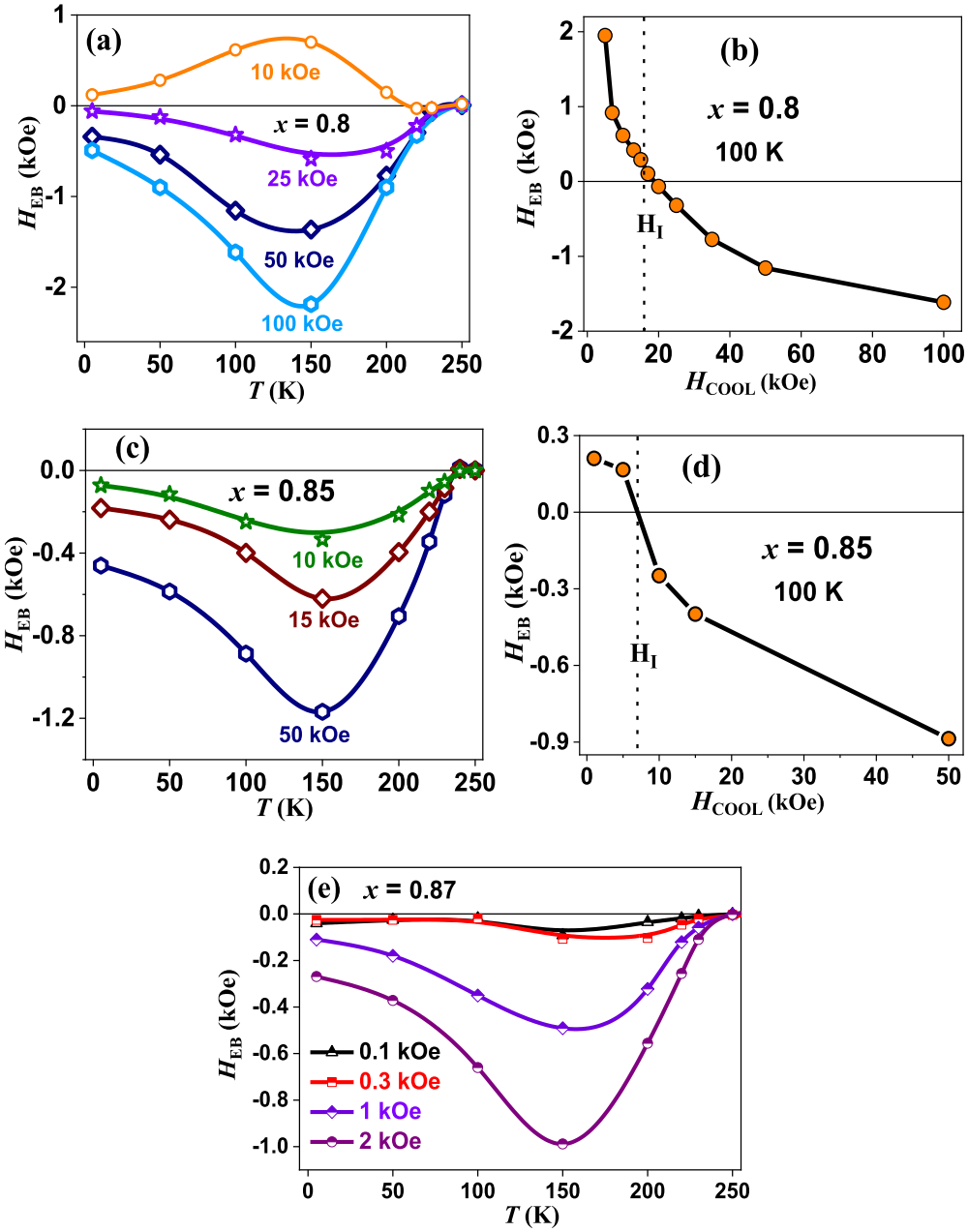

FIG. 5. Thermal variation of H_{EB} for (a) $x = 0.8$, (c) $x = 0.85$, and (e) $x = 0.87$ under different H_{COOL}s. Variation of H_{EB} with H_{COOL} at 100 K for (b) $x = 0.8$ and (d) $x = 0.85$.

D. Magnetic neutron diffraction

Since the $La_{1-x}Pr_xCrO_3$ ($x = 0.8 - 0.9$) compounds show the fascinating phenomena of NM and EB, so it is quite essential to investigate the magnetic ground state of these compounds using a microscopic neutron diffraction (ND) technique. The ND data for all compounds over the temperature range of 5–300 K under a zero magnetic field have been recorded. Since all compounds exhibit similar ND patterns, therefore, the ND data for only $x = 0.8$ are shown in Fig. 6(a). It is evident from the ND patterns at $T < T_N$ that {(011)(110)} Bragg peaks are purely magnetic, while {(211)(031) and (132)(310)} Bragg peaks have nuclear contribution also. All magnetic Bragg peaks are indexed with the propagation vector $\mathbf{k} = (000)$. The Rietveld refinement on the ND data has been carried out by considering both nuclear (space group: *Pnma*) and magnetic phases, and a good agreement has been obtained between the experimental and calculated data with a magnetic reliability factor (R_{mag}) ~ 3 [Fig. 6(b)]. The Rietveld refinement infers that the increment in the intensities of above-mentioned Bragg peaks is accounted by the G_y magnetic ordering of Cr^{3+} spins. Same magnetic model has been used for the Rietveld refinement of ND data of $x = 0.85$, 0.87, and 0.9 compounds (not shown) and the AFM (G_y) component of Cr^{3+} has been estimated. Figure 6(c) shows the temperature variation of AFM Cr^{3+} moment which exhibits a Brillouin-function type dependence.

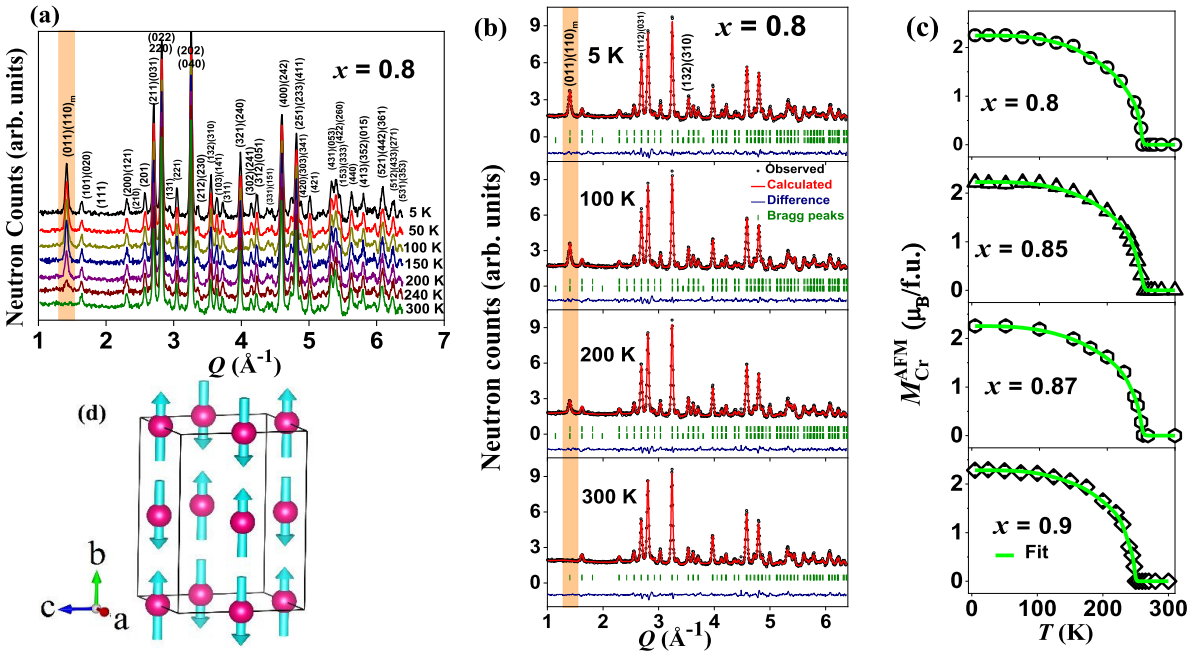

FIG. 6. (a) The ND data of $x = 0.8$ compound at various temperatures plotted as a function of momentum transfer $Q = 4\pi \sin\theta/\lambda$. Here θ is the Bragg angle and λ (=1.094 Å) is the wavelength of incident neutrons. The neutron intensities are shifted vertically upward for clarity. All Bragg peaks are indexed by their respective *hkl* values. (b) Rietveld refined ND patterns of $x = 0.8$ at some selected temperatures. The open (black) symbols show the experimental data, while the solid red line is a Rietveld fit. The difference of these two data is shown by a navy-blue line at the bottom. The vertical bars (olive), i.e., upper (lower) for nuclear (magnetic), represent the positions of Bragg reflections. The purely magnetic {(110)(011)} Bragg peaks are highlighted by the orange color. (c) Thermal variation of the AFM (G_y) Cr^{3+} moment in $La_{1-x}Pr_xCrO_3$ ($x = 0.8$, 0.85, 0.87, and 0.9) compounds. The solid green line shows a fit using molecular-field approach as described in the text. (d) Magnetic structure of these compounds consisting of AFM G_y Cr^{3+} spins.

The temperature-dependent AFM Cr^{3+} moment has been analyzed using the molecular-field approach. According to this approach, the magnetic moment data can be fitted with the following equation, $M_{Cr}^{AFM}(T) = M_S B_S(x)$, where $M_S(T)$ is the saturation magnetization and $B_S(x)$ is the Brillouin function which can be expressed as $B_S(x) = \frac{(2J+1)}{2J}\coth(\frac{2J+1}{2J}x) - \frac{1}{2J}\coth(\frac{1}{2J}x)$, where $x = \frac{gJ\mu_B H}{k_B T}$. The above equation successfully fits the experimental AFM Cr^{3+} moment [solid green line in Fig. 6(c)] and the estimated M_S lies between ~2.2(1) to 2.3(1) μ_B for the present $La_{1-x}Pr_xCrO_3$ compounds, which are close to the free-ion spin-only Cr^{3+} moment (3 μ_B). The magnetic structure of the compounds with AFM G_y ordering of Cr^{3+} spins is shown in Fig. 6(d). Further, it is known that the FM (M_{Cr}) component of the Cr^{3+} is generally very small (~10^{-2}–10^{-5} μ_B) in $RCrO_3$ compounds [27,41], therefore, it could not be detected in the present ND experiments. On the other hand, despite having theoretically large Pr^{3+} magnetic moment (gJ)~2.6–2.9 μ_B for $x = 0.8$–0.9, it could also not be detected in our zero-field ND experiments. It indicates that the Pr^{3+} moment (M_{Pr}) in these compounds is very small and is below the detection limit of the instrument. We may expect the small Pr^{3+} moment if the Pr^{3+} spins are weakly polarized under the Cr^{3+} internal field. However, these small moments are indeed present and an atomistic coupling between them is responsible for the remarkable NM and EB phenomena in the compounds as discussed in the next section.

IV. DISCUSSION

For $RCrO_3$ systems, it is known that the Cr^{3+} atom exhibits canted AFM ordering with both AFM and weak FM (M_{Cr}) moments, and R^{3+} polarizes under the internal field of ordered Cr^{3+} atoms [42]. In this study, we have probed AFM Cr^{3+} moment using a microscopic neutron diffraction technique (Sec. III D), while M_{Cr}, which arises from the canting of AFM ordered Cr^{3+} moments due to the Dzyaloshinskii-Moriya interaction [41,43] and polarized Pr^{3+} moment (M_{Pr}) are estimated using the Cooke's model fit [44] to dc magnetization data. The polarized nature of Pr^{3+} in the present compounds is evident from the neutron depolarization experiments (Sec. III B). Interestingly, the estimated M_{Cr} and M_{Pr} moments and their orientations with respect to internal (H_I) and external (H) applied magnetic fields not only explain the NM, its elusive disappearance for $x > 0.87$ and anomalous M behavior but also provide an insight into the remarkable inverse and conventional EB results.

The dc magnetization data of $La_{1-x}Pr_xCrO_3$ ($x = 0.8$, 0.85, 0.87, and 0.9) compounds under $H = 100$ Oe [Fig. 7(a)] are fitted using the following expression of the Cooke's model:

$$M = M_{Cr} + \frac{C(H + H_I)}{T + \theta} \quad (2)$$

and the parameters M_{Cr}, H_I, and θ are estimated. In the above expression, the second term corresponds to M_{Pr}; $C = xC_{Pr}$ is

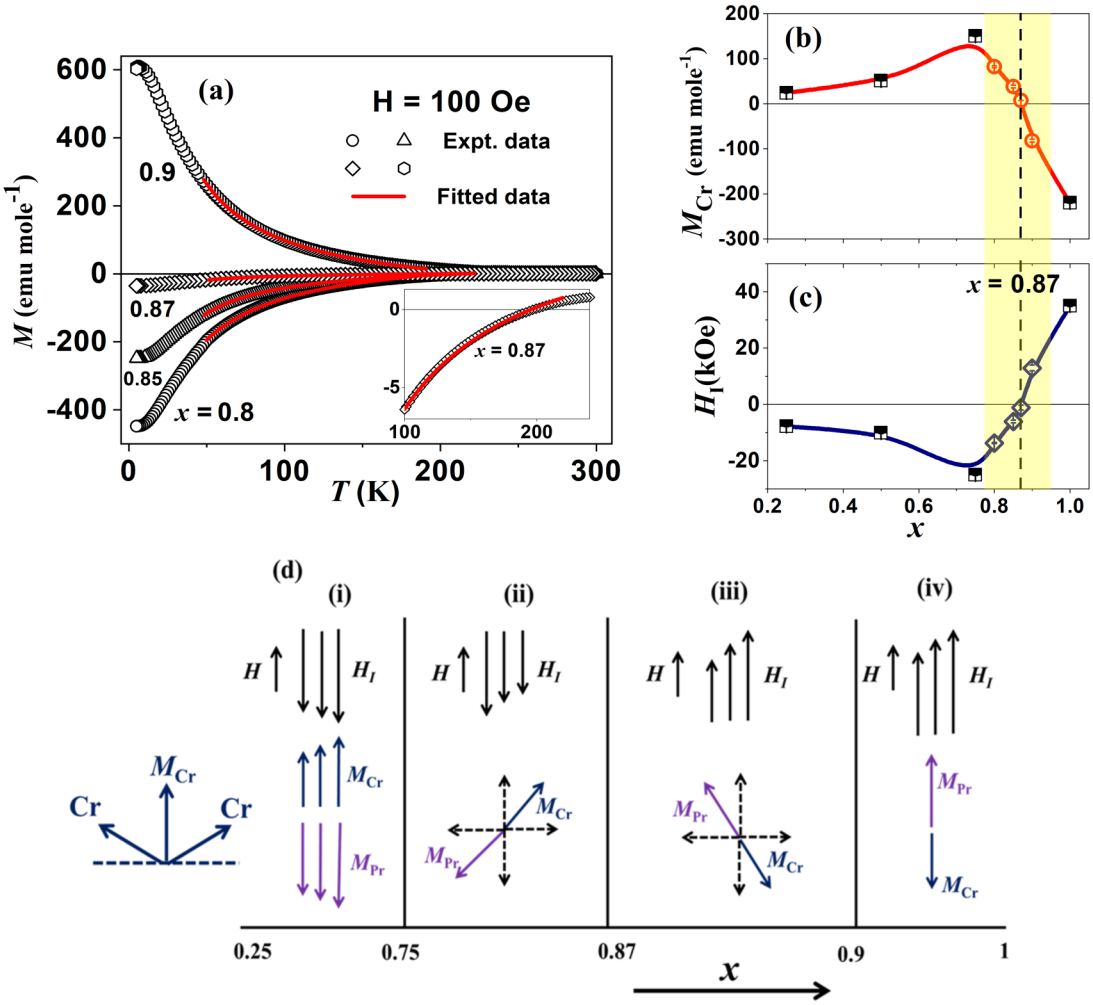

FIG. 7. (a) The M vs T data (open symbols) under $H = 100$ Oe for $x = 0.8$, 0.85, 0.87, 0.9 compounds and fitted curves (red) using the Cooke's model [Eq. (2)]. Inset shows the zoomed view for $x = 0.87$. The x dependence of (b) M_{Cr} and (c) H_I, derived from the Cooke's model. The $0.8 \leqslant x \leqslant 0.9$ range is yellow highlighted. Black squared symbol data are taken from Ref. [28]. (d) Schematic depicts the orientations of M_{Cr} and M_{Pr} moments with respect to the external (H) and internal (H_I) magnetic fields for different x in $La_{1-x}Pr_xCrO_3$ compounds. The dotted arrows in (d) serve as a reference for M_{Cr} and M_{Pr} moments with respect to H and H_I. The drawn moments and magnetic fields in (d) are not shown to scale.

the Curie constant with $C_{Pr} = 1.602$ emu-K/mole-Oe [27], H and H_I are the externally applied and internal magnetic fields, respectively, and θ is the Weiss constant. The derived θ's ~ 4.9 (9), 3.2 (1), 7.7 (1), and 4.3 (1) K for the respective compounds indicate the dominant antiferromagnetic interactions. The variation of the derived M_{Cr} and H_I as a function of x is shown in Figs. 7(b) and 7(c). The M_{Cr} and H_I for $x =$ 0.25, 0.5, 0.75, and 1 compounds are also shown, taken from Ref. [28]. Similar to maximum $|M|$ for $x = 0.75$ [Fig. 1(e)], the compound also shows the highest positive M_{Cr} and negative H_I compared to $x = 0.25$ and 0.5 compounds. However, it is worthy to note from Figs. 7(b) and 7(c) that for $x > 0.75$, M_{Cr} ($|H_I|$) start to decrease, changes its sign from positive (negative) to negative (positive) across $x = 0.87$, consistent with the M data shown in Fig. 1(e). Similar to the $x = 0.8$ and 0.85, positive M_{Cr} and negative H_I, however small, are found for $x = 0.87$. The positive and negative M_{Cr} indicate the FM Cr^{3+} alignment in the same and opposite direction, respectively, relative to the H. The negative H_I ($> H$) for $x = 0.8$, 0.85, and 0.87 compounds make M_{Pr} negative indicating its alignment opposite to H as well as M_{Cr} (aligned along H). The dominance of M_{Pr} over M_{Cr} (aligned along H) below T_{COMP} results in the NM in $x = 0.8$, 0.85, and 0.87 compounds. On the other hand, for the $x = 0.9$ compound, the positive H_I indicates that the positive magnetization in these compounds is dominated by M_{Pr} polarized along H, while (negative) M_{Cr} is opposite to both.

Now we explain the disappearance of NM for $x > 0.87$ and anomalous M behavior in $La_{1-x}Pr_xCrO_3$ compounds. Fig. 7(d)(i–iv) depicts a schematic showing the orientations of M_{Cr} and M_{Pr} as a function of x. For $0.25 \leqslant x \leqslant 0.75$, $|M_{Cr}|$ increases with x leading to the increase in $|H_I|$ [Figs. 7(b) and 7(c)] which in turn increases the $|M_{Pr}|$. As $|M_{Pr}|$ is larger than $|M_{Cr}|$, it causes the net $|M|(= |M_{Pr}| - |M_{Cr}|)$ to increase with x [Fig. 1(e)]. For $0.75 < x < 0.87$, a decrease in $|H_I|$ [Fig. 7(c)] causes some of the M_{Pr} spins to rotate along the direction of H. However, both M_{Cr} and M_{Pr} are antiferromagnetically coupled by a large $|H_I|$ of the order of

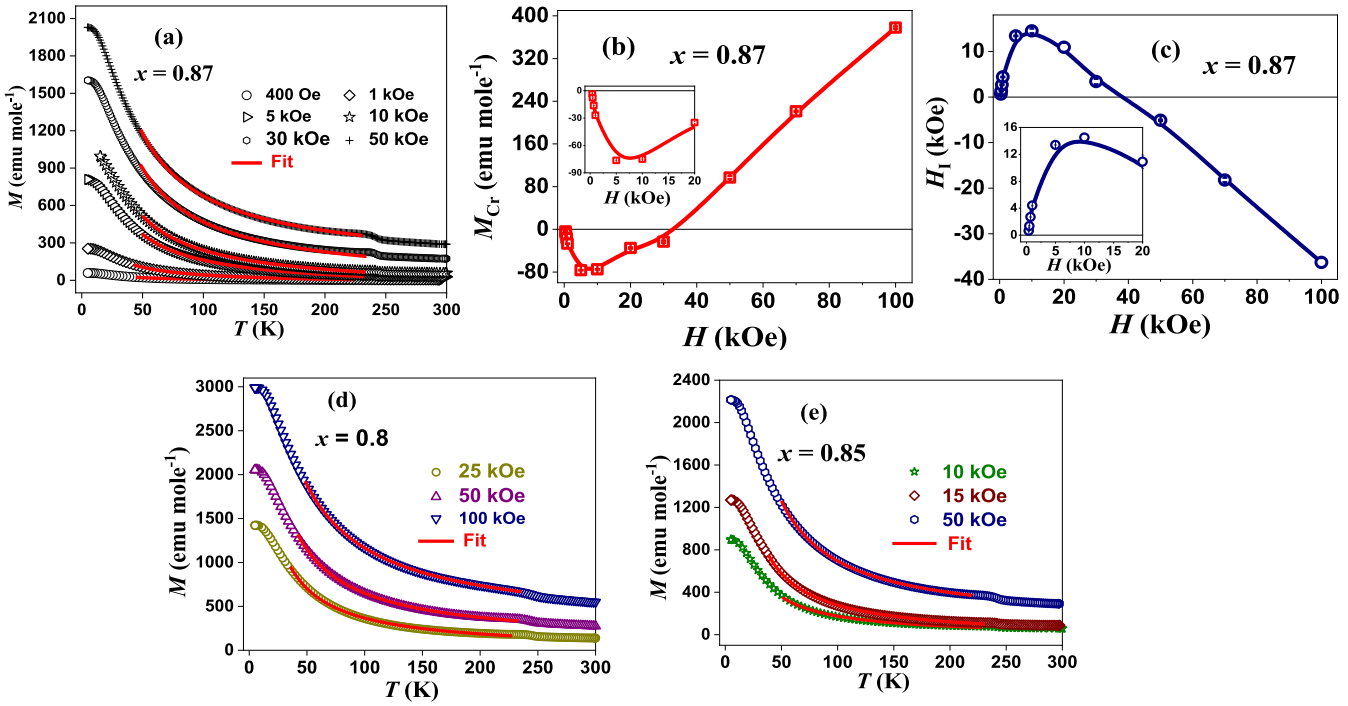

FIG. 8. Fitted (red line) M vs T data (open symbols) for (a) $x = 0.87$, (d) $x = 0.8$, and (e) $x = 0.85$ compounds using the Cooke's model. The H variation of (b) M_{Cr} and (c) H_I for the $x = 0.87$ compound. Insets show the enlarged view of M_{Cr} and H_I in the low-H region.

~kOe, therefore, the coupled sublattices will rotate simultaneously. Consequently, the net (M_{Cr} and M_{Pr}) moment in the direction of H decreases, which in turn decreases the $|M|$ [see Fig. 1(e) for M behavior and Fig. 7(d)(ii) for schematic]. For $x = 0.87$, M_{Pr} and M_{Cr} moment orientations are such that they almost compensate each other, resulting in the smallest $|M|$ for the compound. The almost compensated magnetic domains are also evident from the neutron depolarization experiments (Fig. 3). Further for $x > 0.87$, the positive H_I makes net effective magnetic field ($H + H_I$) positive which causes more and more M_{Pr} spins to rotate further along the direction of H or equivalently along $H_I + H$, leading to the disappearance of NM and hence positive M for $x > 0.87$ [Fig. 1(e)]. The orientations of M_{Cr} and M_{Pr} for $x > 0.87$ compounds are shown in Fig. 7(d) (iii and iv).

It is interesting to note here that the polarization of Pr^{3+} spins under the internal field of Cr^{3+} plays an important role not only in bringing the NM in these compounds but also in NM disappearance for $x > 0.87$. It is also interesting to compare the magnetization results of present $La_{1-x}Pr_xCrO_3$ compounds with the literature reported $La_{1-x}Ce_xCrO_3$ compounds [45]. These compounds show the NM phenomenon for $0.8 \leqslant x \leqslant 1$ where it was explained by considering the dominant polarized Ce^{3+} moment, aligned opposite to the Cr^{3+} moment under its internal field. For the intermediate compositions ($0.5 < x < 0.8$), only a downturn in the field-cooled magnetization data with decreasing temperature, without NM, was observed, also suggesting a finite contribution of polarized Ce^{3+} moment to the field-cooled magnetization. However, for $x \leqslant 0.5$, $La_{1-x}Ce_xCrO_3$ compounds show neither NM nor downturn in the field-cooled magnetization data, implying the effect of polarized Ce^{3+} moment to the field-cooled magnetization is negligible. This comparison indicates that the polarized Pr^{3+} moment is indeed responsible in deciding the interesting magnetic behavior of all compounds of $La_{1-x}Pr_xCrO_3$ series. Further, we have also fitted the present H-dependent M data for $x = 0.8$ [Fig. 2(a)] and 0.85 [Fig. 2(b)] compounds below the T_{COMP} with the Cooke's model (fitted data are not shown) and parameters $M_{Cr} \sim$ 70.54–98, 32.26–45.13 emu mole^{-1} and $|H_I| \sim$ 11.5–15.7, 5.2–7 kOe, respectively, are estimated. The θ's~4.9 and 3.2 K are kept fixed for the fitting.

Now we turn our attention to explain the interesting EB results in $La_{1-x}Pr_xCrO_3$ ($x = 0.8 - 0.9$) compounds (Figs. 4 and 5). To understand these EB results, it is necessary to understand the orientation of M_{Cr} and M_{Pr} moments with respect to H in these compounds. We first focus on EB results of $x = 0.87$ compound. The M vs T curves under various H ($\geqslant$ 300 Oe) for this compound are fitted using the Cooke's model [Eq. (2), while some of them are shown in Fig. 8(a), and the derived M_{Cr} and H_I are plotted in Figs. 8(b) and 8(c). The $\theta \sim 7.7$ K is kept fixed for the fitting. The fitted results reveal negative values of M_{Cr} and positive values of H_I, similar to $x = 0.9$, for $H \leqslant 30$ kOe, while reverse polarities are observed for $H > 30$ kOe. We call this field as critical magnetic field (H_{ct}). Since H_I is positive for $H \leqslant H_{ct}$, M_{Pr} aligns along H_I (also along H) and M_{Cr} opposite to it in the beginning to the M-H cycle. Therefore, during the magnetic field cycle of $+H_{max}$ to $-H_{max}$ in a hysteresis loop, AFM coupling between M_{Cr} and M_{Pr} will hinder the rotation of dominant M_{Pr} along the negative direction of applied H. This occurs because a positive magnetization state is energetically favorable for the compound, resulting in higher H_{C1}. Whereas an easy switching of the M_{Pr} along the direction of positive magnetic field

while changing the magnetic field from $-H_{max}$ (=50 kOe) to $+H_{max}$ (=50 kOe) in a hysteresis loop makes H_{C2} smaller. Consequently, a conventional (negative H_{EB}) EB is observed. Similar explanation also holds for explaining conventional EB in $x = 0.9$ [Fig. 4(b)] owing to similar orientations of M_{Cr} and M_{Pr} in the compound. Now the question is what happens to the orientations of two spin moments in $x = 0.87$ when measured under H (=50, 70, and 100 kOe) > H_{ct}, and what would be its consequences on the EB sign. It can be seen from Figs. 8(b) and 8(c) that for $H = 50$, 70, and 100 kOe, the derived M_{Cr} is positive and H_I is negative. Since for these field values, H is much larger than the $|H_I|$, it provides high Zeeman energy to M_{Pr} thus preventing it from aligning opposite to positive M_{Cr}. This leads to a FM coupling between these moments and hence resulting again a conventional (negative H_{EB}) EB.

According to the literature [13,14], it is the only FM interfacial coupling which is responsible for the conventional EB in heterostructures. However, our study shows that it is not only the FM coupling between the moments which brings the conventional EB but AFM coupling can also be respsonsible for the same effect in single-phase homogeneous magnetic systems. In the next paragraph, we show that the AFM and FM couplings between M_{Cr} and M_{Pr} moments can also lead to conventional EB in $x = 0.8$ and 0.85 compounds which supports the conventional EB results for $x = 0.87$ compound.

Now we focus on the EB results of $x = 0.8$ and 0.85 compounds. We recall from Figs. 4(b) and 5(a)–5(d) that these compounds exhibit the sign reversal of H_{EB} from positive ($H_{COOL} < |H_I|$) to negative ($H_{COOL} > |H_I|$). Similar tuned H_{EB} behavior is reported in the literature for $x = 0.85$, where authors explained positive and negative H_{EB} by considering the AFM and FM couplings between M_{Pr} and M_{Cr}, respectively [30]. Our results also infer that an AFM coupling leads to positive H_{EB} in both $x = 0.8$ and 0.85 compounds, and it can be explained by the mechanism described above for $x = 0.87$. The only difference is that for $x = 0.8$ and 0.85, when $H_{COOL} < |H_I|$ (~15.7 kOe for $x = 0.8$ and ~7 kOe for $x = 0.85$), where NM state is favorable, M_{Cr} aligns along the direction of H and M_{Pr} opposite to it in the beginning of M-H cycle [28]. This alignment leads to positive H_{EB} in both the compounds [Figs. 4(b) and 5(a)–5(d)]. Further, similar to the case of $x = 0.87$, both FM and AFM couplings between M_{Pr} and M_{Cr} moments can contribute to negative H_{EB} in $x = 0.8$ and 0.85 compounds, rather than only FM coupling, as reported in the literature for $x = 0.85$ [30]. To explain the present negative H_{EB} results for $x = 0.8$ and 0.85 [Figs. 5(a)–5(d)], we have fitted their M vs T data recorded under $H = 25$, 50, and 100 kOe for $x = 0.8$ [Fig. 8(d)], and $H = 10$, 15, and 50 kOe for $x = 0.85$ [Fig. 8(e)], using the Cooke's model. Interestingly, for $x = 0.8$ under H (= 50 and 100 kOe) and 0.85 under $H = 50$ kOe, the derived M_{Cr} and H_I results align well with those for $x = 0.87$ under H (> H_{ct}), revealing a FM coupling and resulting in negative H_{EB} in the compounds. While for $x = 0.8$ under $H = 25$ kOe and $x = 0.85$ under $H = 10$ and 15 kOe, an AFM coupling between dominant positive M_{Pr} and negative M_{Cr} is observed, consistent with $x = 0.87$ for $H < H_{ct}$, again leads to a negative H_{EB}. Thus, our study reveals that both AFM and FM couplings between two moments can be responsible for the observed negative H_{EB} in $x = 0.8$, 0.85, and 0.87 compounds. We would like to mention

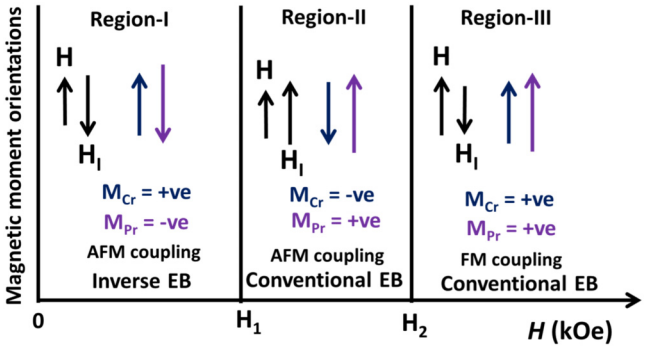

FIG. 9. Schematic diagram showing spin orientations of M_{Cr} (navy blue) and M_{Pr} (violet) moments with respect to H and H_I in the $La_{1-x}Pr_xCrO_3$ ($x = 0.8$–0.9) compounds. Here H_1 and H_2 denote the critical magnetic fields. The drawn variables *viz.* moments and magnetic fields are not on an absolute scale.

that the AFM coupling at high magnetic fields, where the rare-earth sublattice aligns along H and opposite to transition-metal sublattice, is unusual and rare but has also been reported in $ErFeO_3$ single crystals [46,47], which are isostructural to the present compounds ($H \sim 15$ kOe in Ref. [46] and $H \sim 180$ kOe in Ref. [47]). Further, it may be noted that despite $x = 0.87$ exhibits the NM like to $x = 0.8$ and 0.85, the compound does not show the inverse EB. It may also be noted that the $H_I \sim -600$ Oe for $x = 0.87$ in the NM state is significantly smaller than the $x = 0.8$ ($H_I \sim -15.7$ kOe) and 0.85 ($H_I \sim -7$ kOe) compounds. This may change initial Pr^{3+}-Cr^{3+} coupling [Figs. 7(b) and 7(c)], responsible for NM, during demagnetization process in the hysteresis loop measurements in such a way that results always conventional EB in the $x = 0.87$ compound (as discussed earlier) even in the NM state.

Based on our comprehensive magnetization results, we propose a schematic depicting the orientations of M_{Cr} and M_{Pr} with H in $La_{1-x}Pr_xCrO_3$ ($x = 0.8$–0.9) compounds as shown in Fig. 9. In the low-H region, the inverse EB (in the NM state) is favored with M_{Cr} and M_{Pr} orientations shown in region I. As H is increased (region II) and exceeds a certain critical field (H_1), the M_{Cr} and M_{Pr} moments reorient themselves into a different spin configuration with AFM coupling responsible for conventional EB. Upon further increase of H and above H_2 (region III), the AFM coupling between the moments weakens and it changes into FM coupling which also contributes to conventional EB.

In brief, our comprehensive EB study demonstrates that $La_{1-x}Pr_xCrO_3$ compounds provide a unique platform to study concurrent occurrences of inverse and conventional EB, which are otherwise rarely observed, based on the AFM and FM/AFM coupling, respectively, between M_{Cr} and M_{Pr} moments. Since $La_{1-x}Pr_xCrO_3$ compounds exhibit remarkable NM and EB phenomena, thus making these useful for thermomagnetic switches and thermal-assisted magnetic random access memory devices. However, an easy magnetization switching feature of critical composition $x = 0.87$ makes this compound further promising for several advanced technological applications. For instance, the magnetization switching

at a much smaller field (∼300 Oe) requires less energy for writing and erasing magnetic states, making this compound an ideal candidate for low-power spintronic memory devices. Furthermore, this feature may also have implications for highly sensitive magnetic sensors and ultrafast magnetic switching devices.

V. COMMENT ON POLARIZED Pr^{3+}

We finally give a discussion on the polarization of Pr^{3+} spins under the internal field of Cr^{3+} in $La_{1-x}Pr_xCrO_3$ compounds and its comparison with other $R_{1-x}R'_xTMO_3$ (R and R' are two different rare earths and TM is a transition metal) [37,48,49] and Pr^{3+}-based compounds [50,51]. Barbosa *et al.* explained the NM phenomenon in $Nd_{1-x}Pr_xCrO_3$ ($x = 0.15$ to 0.6) compounds by considering the AFM coupling between FM Cr^{3+} and polarized Nd^{3+} spins [37]. They completely excluded the polarization of Pr^{3+} spins owing to the large crystal-field splitting ∼48 K between the ground state and first-excited energy levels of the Pr^{3+} ions in $PrCrO_3$ and considered the Pr^{3+} spins in paramagnetic state. Contrary to $Nd_{1-x}Pr_xCrO_3$, $Nd_{1-x}Dy_xCrO_3$ ($x = 0.2$ and 0.33) [16,40] compounds do not show the NM phenomenon indicating the crucial role of Pr^{3+} in bringing the NM in $Nd_{1-x}Pr_xCrO_3$. Further, in $Y_{1-x}Pr_xCrO_3$ [48] and $Gd_{0.5}Pr_{0.5}MnO_3$ [49] compounds, authors also considered the polarization of Pr^{3+} under the internal field of Cr^{3+} and Mn^{3+}, respectively, to explain the NM, consistent with our present study on $La_{1-x}Pr_xCrO_3$. Here it is worthy to note that both end members of $Y_{1-x}Pr_xCrO_3$ and $Gd_{0.5}Pr_{0.5}MnO_3$ compounds do not show the NM phenomenon further supporting the role of polarized Pr^{3+} in bringing the NM in these two compounds. Furthermore, in some Pr-based intermetallic compounds, the polarized or induced moment of Pr is observed, as indicated by the Schottky anomaly in heat capacity data, provided that the crystal field splitting between ground and first excited levels of Pr is large (∼90 K) [50,51]. Therefore, more investigations are required on Pr^{3+}-based compounds to get insight of the exact cause of its polarization and hence its role in deciding the magnetic properties of a given magnetic material. At the same time, we cannot neglect the polarization of Pr^{3+} in the present non-NM $La_{1-x}Pr_xCrO_3$ ($x > 0.87$) compounds also. This is because if Pr^{3+} spins are in paramagnetic state without any polarization, then there would not be any depolarization of the polarized neutron beam (Fig. 3) as no significant change in the FM Cr^{3+} moment is expected with increasing Pr^{3+} concentration causing itself to depolarize the incident-polarized neutron beam [28]. Since the observed P_f variation [Fig. 3(b)] is similar to that of H_I [see highlighted part of Fig. 7(c)], it further suggests the polarization of Pr^{3+} in these $La_{1-x}Pr_xCrO_3$ compounds. The polarization of Pr^{3+} under the internal field of Cr^{3+} or Fe^{3+}/Cr^{3+} is reported in other non-NM orthochromite compounds $(Gd/Pr)CrO_3$, $Pr_{0.5}Eu_{0.5}CrO_3$, $Pr_{0.5}Y_{0.5}CrO_3$, and $PrFe_{0.5}Cr_{0.5}O_3$ [52,53].

VI. SUMMARY AND CONCLUSIONS

The comprehensive investigations of two magnetic phenomena involving NM and EB have been carried out on $La_{1-x}Pr_xCrO_3$ ($x = 0.8$ –0.9) compounds. Despite all compounds belonging to the same *Pnma* space group, notable and interesting magnetic behaviors are observed with varying Pr^{3+} composition, temperature, and, more importantly, with varying magnetic field. The dc magnetization study reveals several striking features: (i) NM phenomenon is observed in $x = 0.8$, 0.85, 0.87 but not in $x = 0.9$. (ii) An anomalous magnetization behavior with a minimum magnetization for $x = 0.87$ is noted, despite its higher Pr^{3+} concentration compared to $x = 0.8$ and 0.85. (iii) Remarkably, both inverse and conventional EB are observed in $x = 0.8$ and 0.85, while only conventional EB is present in $x = 0.87$ and 0.9. Interestingly, all these results are explained by considering the competition between the polarized Pr^{3+} (M_{Pr}) and weak ferromagnetic component of canted Cr^{3+} (M_{Cr}) moments derived from the Cooke's model fit, indicating that both phenomena share the same underlying physics origin. The AFM Cr^{3+} moments derived from the neutron diffraction for all compounds are fitted using the molecular-field approach. The most notable conclusion from this study is that AFM as well as FM coupling can lead to the conventional EB in the compounds, in contrast to the previously understood model, which only considered FM coupling. Furthermore, the detailed and comprehensive study also demonstrates that both NM and EB are indeed correlated with each other and thus strengthen the subject knowledge of these two fascinating phenomena in condensed matter physics research area. The intriguing features of NM and EB reversals with temperature and magnetic field in the present $La_{1-x}Pr_xCrO_3$ compounds are reminiscent of similar manipulations of magnetization and EB with magnetic field, electric field, current, and strain in various heterostructures, facilitating their applications in spintronic devices [54–56].

ACKNOWLEDGMENTS

D.G. acknowledges the postdoctoral funding from the European Union's Horizon 2020 research and innovation programme under the Marie Skłodowska-Curie Grant Agreement No. 101034266. D.G. also acknowledges B. Veltel for his assistance in physical property measurements performed at the Physics Lab of the Heinz Maier-Leibnitz Zentrum (MLZ). S.M.Y. acknowledges the financial assistance from SERB, Department of Science and Technology, Government of India under the J. C. Bose fellowship program (Grant No. JCB/2023/000014).

DATA AVAILABILITY

The data that support the findings of this article are not publicly available. The data are available from the authors upon reasonable request.

[1] A. Kumar and S. M. Yusuf, The phenomenon of negative magnetization and its implications, Phys. Rep. **556**, 1 (2015).

[2] V. Kuncser, M. Valeanu, G. Schinteie, G. Filoti, I. Mustata, C. P. Lungu, A. Anghel, H. Chiriac, R. Vladoiu, and J. Bartolome, Exchange bias and spin valve systems with Fe–Mn antiferromagnetic pinning layers, obtained by the thermoionic vacuum arc method, J. Magn. Magn. Mater. **320**, e226 (2008).

[3] J. C. S. Kools, Exchange-biased spin-valves for magnetic storage, IEEE Trans. Magn. **32**, 3165 (1996).

[4] X. He, Y. Wang, N. Wu, A. N. Caruso, E. Vescovo, K. D. Belashchenko, P. A. Dowben, and C. Binek, Robust isothermal electric control of exchange bias at room temperature, Nat. Mater. **9**, 579 (2010).

[5] C. Binek, A. Hochstrat, X. Chen, P. Borisov, W. Kleemann, and B. Doudin, Electrically controlled exchange bias for spintronic applications, J. Appl. Phys. **97**, 10C514 (2005).

[6] W. H. Meiklejohn and C. P. Bean, New magnetic anisotropy, Phys. Rev. **102**, 1413 (1956).

[7] F. G. Silva, J. Depeyrot, Y. L. Raikher, V. I. Stepanov, I. S. Poperechny, R. Aquino, G. Ballon, J. Geshev, E. Dubois, and R. Perzynski, Exchange-bias and magnetic anisotropy fields in core–shell ferrite nanoparticles, Sci. Rep. **11**, 5474 (2021).

[8] B. Leszczyński, G. C. Hadjipanayis, A. A. El-Gendy, K. Załęski, Z. Śniadecki, A. Musiał, M. Jarek, S. Jurga, and A. Skumiel, The influence of oxidation process on exchange bias in egg-shaped FeO/Fe_3O_4 core/shell nanoparticles, J. Magn. Magn. Mater. **416**, 269 (2016).

[9] F. Huang, X. Xu, X. Lu, M. Zhou, H. Sang, and J. Zhu, The exchange bias behavior of $BiFeO_3$ nanoparticles with natural core-shell structure, Sci. Rep. **8**, 2311 (2018).

[10] E. Maniv, R. A. Murphy, S. C. Haley, S. Doyle, C. John, A. Maniv, S. K. Ramakrishna, Y.-L. Tang, P. Ercius, R. Ramesh *et al.*, Exchange bias due to coupling between coexisting antiferromagnetic and spin-glass orders, Nat. Phys. **17**, 525 (2021).

[11] A. Hoffmann, M. Grimsditch, J. E. Pearson, J. Nogués, W. A. A. Macedo, and I. K. Schuller, Tailoring the exchange bias via shape anisotropy in ferromagnetic/antiferromagnetic exchange-coupled systems, Phys. Rev. B **67**, 220406(R) (2003).

[12] M. Ali, P. Adie, C. H. Marrows, D. Greig, B. J. Hickey, and R. L. Stamps, Exchange bias using a spin glass, Nat. Mater. **6**, 70 (2007).

[13] J. Nogués, D. Lederman, T. J. Moran, and I. K. Schuller, Positive Exchange Bias in FeF_2-Fe Bilayers, Phys. Rev. Lett. **76**, 4624 (1996).

[14] J. Nogués, C. Leighton, and I. K. Schuller, Correlation between antiferromagnetic interface coupling and positive exchange bias, Phys. Rev. B **61**, 1315 (2000).

[15] P. Gupta and D. Pal, Spin induced exchange bias and lattice modulation in $Nd_{1-x}Eu_xCrO_3$, J. Phys.: Condens. Matter **33**, 135806 (2021).

[16] A. McDannald, C. R. de la Cruz, M. S. Seehra, and M. Jain, Negative exchange bias in single-phase $Dy_{1-x}Nd_xCrO_3$ induced by Nd doping, Phys. Rev. B **93**, 184430 (2016).

[17] A. Kumar, S. K. Giri, T. K. Nath, C. Ritter, and S. M. Yusuf, Investigation of magnetic ordering and origin of exchange-bias effect in doped manganite, $Sm_{0.4}Ca_{0.6}MnO_3$, J. Appl. Phys. **128**, 203901 (2020).

[18] D. Garg, A. Kumar, and S. M. Yusuf, Unraveling intricate magnetic behavior involving negative magnetization and exchange-bias in $ErFe_{0.5}Co_{0.5}O_3$, Phys. Rev. B **110**, 104401 (2024).

[19] Deepak, A. Kumar, S. M. Yusuf, and E. V. Sampathkumaran, Insight into the negative magnetization and anomalous exchange-bias in $DyFe_5Al_7$ through neutron depolarization and neutron diffraction studies, J. Phys.: Condens. Matter **35**, 065802 (2023).

[20] Deepak, A. Kumar, and S. M. Yusuf, Intertwined magnetization and exchange bias reversals across compensation temperature in $YbCrO_3$ compound, Phys. Rev. Mater. **5**, 124402 (2021).

[21] B. Dalal, X. Kang, Y. Matsushita, A. A. Belik, Y. Tsujimoto, and K. Yamaura, Inverse exchange bias effects and magnetoelectric coupling of the half-doped perovskite-type chromites $Gd_{0.5}Sr_{0.5}CrO_3$ and $Gd_{0.5}Ca_{0.5}CrO_3$, Phys. Rev. B **106**, 104425 (2022).

[22] I. Fita, V. Markovich, A. S. Moskvin, A. Wisniewski, R. Puzniak, P. Iwanowski, C. Martin, A. Maignan, R. E. Carbonio, M. U. Gutowska *et al.*, Reversed exchange-bias effect associated with magnetization reversal in the weak ferrimagnet $LuFe_{0.5}Cr_{0.5}O_3$, Phys. Rev. B **97**, 104416 (2018).

[23] L. Wang, G. H. Rao, X. Zhang, L. L. Zhang, S. W. Wang, and Q. R. Yao, Reversals of magnetization and exchange-bias in perovskite chromite $TmCrO_3$, Ceram. Int. **42**, 10171 (2016).

[24] I. L. Prejbeanu, M. Kerekes, R. C. Sousa, H. Sibuet, O. Redon, B. Dieny, and J. P. Nozières, Thermally assisted MRAM, J. Phys.: Condens. Matter **19**, 165218 (2007).

[25] C. De, A. K. Nayak, M. Nicklas, and A. Sundaresan, Magnetic compensation-induced sign reversal of exchange bias in a multi-glass perovskite $SmFeO_3$, Appl. Phys. Lett. **111**, 182403 (2017).

[26] D. Deng, J. Zheng, D. Yu, B. Wang, D. Sun, M. Avdeev, Z. Feng, C. Jing, B. Lu, W. Ren *et al.*, Cooling field tuned magnetic phase transition and exchange bias-like effect in $Y_{0.9}Pr_{0.1}CrO_3$, Appl. Phys. Lett. **107**, 102404 (2015).

[27] Deepak, A. Kumar, and S. M. Yusuf, Correlation of exchange-bias effect with negative magnetization in perovskite compound, $La_{0.5}Pr_{0.5}CrO_3$, J. Appl. Phys. **127**, 213903 (2020).

[28] Deepak, A. Kumar, A. K. Bera, and S. M. Yusuf, Correlated negative magnetization, exchange bias, and electrical properties in $La_{1-x}Pr_xCrO_3$, Phys. Rev. Mater. **6**, 074405 (2022).

[29] K. Yoshii, A. Nakamura, Y. Ishii, and Y. Morii, Magnetic Properties of $La_{1-x}Pr_xCrO_3$, J. Solid State Chem. **162**, 84 (2001).

[30] K. Yoshii, Positive exchange bias from magnetization reversal in $La_{1-x}Pr_xCrO_3$ ($x \sim 0.7$–0.85), Appl. Phys. Lett. **99**, 142501 (2011).

[31] See Supplemental Material at http://link.aps.org/supplemental/10.1103/PhysRevMaterials.9.054406 for details of the x-ray diffraction data of $La_{1-x}Pr_xCrO_3$ ($x = 0.8$, 0.85, 0.87, and 0.9) compounds at room temperature, dc magnetization data of $x = 0.9$, and EB results of all compounds under different Hcool.

[32] H. Rietveld, A profile refinement method for nuclear and magnetic structures, J. Appl. Crystallogr. **2**, 65 (1969).

[33] J. Rodríguez-Carvajal, Recent advances in magnetic structure determination by neutron powder diffraction, Phys. B (Amsterdam) **192**, 55 (1993).

[34] J. Prado-Gonjal, R. Schmidt, J.-J. Romero, D. Ávila, U. Amador, and E. Morán, Microwave-assisted synthesis, microstructure, and physical properties of rare-earth chromites, Inorg. Chem. **52**, 313 (2013).

[35] O. Halpern and T. Holstein, On the Passage of Neutrons Through Ferromagnets, Phys. Rev. **59**, 960 (1941).

[36] S. M. Yusuf, M. Sahana, K. Dörr, U. K. Rößler, and K. H. Müller, Effect of Ga doping for Mn on the magnetic properties of $La_{0.67}Ca_{0.33}MnO_3$, Phys. Rev. B **66**, 064414 (2002).

[37] C. C. S. Barbosa, J. R. Jesus, E. M. Bittar, L. Mendonça-Ferreira, S. G. Mercena, M. H. Carvalho, P. G. Pagliuso, J. G. S.

Duque, and C. T. Meneses, Coexistence of positive and negative exchange bias effect in Pr-doped $NdCrO_3$ samples, J. Alloys Compd. **939**, 168629 (2023).

[38] B. B. Dash and S. Ravi, Magnetization reversal and exchange bias study in bulk $Gd_{1-x}Y_xCrO_3$ ($x = 0.0 - 1.0$), J. Magn. Magn. Mater. **461**, 91 (2018).

[39] P. K. Manna, S. M. Yusuf, R. Shukla, and A. K. Tyagi, Coexistence of sign reversal of both magnetization and exchange bias field in the core-shell type $La_{0.2}Ce_{0.8}CrO_3$ nanoparticles, Appl. Phys. Lett. **96**, 242508 (2010).

[40] J. R. Jesus, F. Garcia, J. G. S. Duque, and C. T. Meneses, Study of exchange bias in single-phase $Dy_{0.2}Nd_{0.8}CrO_3$, J. Alloys Compd. **779**, 577 (2019).

[41] I. Dzyaloshinsky, A thermodynamic theory of "weak" ferromagnetism of antiferromagnetics, J. Phys. Chem. Solids **4**, 241 (1958).

[42] T. Yamaguchi, Theory of spin reorientation in rare-earth orthochromites and orthoferrites, J. Phys. Chem. Solids **35**, 479 (1974).

[43] T. Moriya, Anisotropic superexchange interaction and weak ferromagnetism, Phys. Rev. **120**, 91 (1960).

[44] A. H. Cooke, D. M. Martin, and M. R. Wells, Magnetic interactions in gadolinium orthochromite, $GdCrO_3$, J. Phys. C Solid State Phys. **7**, 3133 (1974).

[45] R. Shukla, J. Manjanna, A. K. Bera, S. M. Yusuf, and A. K. Tyagi, $La_{1-x}Ce_xCrO_3$ ($0.0 \leqslant x \leqslant 1.0$): A new series of solid solutions with tunable magnetic and optical properties, Inorg. Chem. **48**, 11691 (2009).

[46] I. Fita, R. Puzniak, E. E. Zubov, P. Iwanowski, and A. Wisniewski, Temperature-driven spin switching and exchange bias in the $ErFeO_3$ ferrimagnet, Phys. Rev. B **105**, 094424 (2022).

[47] X. X. Zhang, Z. C. Xia, Y. J. Ke, X. Q. Zhang, Z. H. Cheng, Z. W. Ouyang, J. F. Wang, S. Huang, F. Yang, Y. J. Song *et al.*, Magnetic behavior and complete high-field magnetic phase diagram of the orthoferrite $ErFeO_3$, Phys. Rev. B **100**, 054418 (2019).

[48] A. Durán, R. Escamilla, R. Escudero, F. Morales, and E. Verdín, Reversal magnetization, spin reorientation, and exchange bias in $YCrO_3$ doped with praseodymium, Phys. Rev. Mater. **2**, 014409 (2018).

[49] S. Biswas and S. Pal, Effect of Gd/Nd doping on the magnetic properties of $PrMnO_3$, Phys. Scr. **90**, 065805 (2015).

[50] V. K. Anand, D. T. Adroja, and A. D. Hillier, Magnetic and transport properties of $PrRhSi_3$, J. Phys.: Condens. Matter **25**, 196003 (2013).

[51] V. K. Anand, D. T. Adroja, A. Bhattacharyya, A. D. Hillier, J. W. Taylor, and A. M. Strydom, Investigations of the singlet ground state system: $PrIrSi_3$, J. Phys.: Condens. Matter **26**, 306001 (2014).

[52] K. Yoshii, Spin rotation, glassy state, and magnetization switching in $RCrO_3$ ($R = La_{1-x}Pr_x$, Gd, and Tm): Reinvestigation of magnetization reversal, J. Appl. Phys. **126**, 123904 (2019).

[53] L. Hou, L. Shi, J. Zhao, R. Tong, and Y. Xin, Insight into the magnetization reversal and exchange bias in $RFe_{0.5}Cr_{0.5}O_3$ ceramics, J. Phys. Chem. C **125**, 7950 (2021).

[54] J. Kang, J. Ryu, J.-G. Choi, T. Lee, J. Park, S. Lee, H. Jang, Y. S. Jung, K.-J. Kim, and B.-G. Park, Current-induced manipulation of exchange bias in IrMn/NiFe bilayer structures, Nat. Commun. **12**, 6420 (2021).

[55] J. Qi, Y. Zhao, Y. Zhang, G. Yang, H. Huang, H. Lyu, B. Shao, J. Zhang, J. Li, T. Zhu *et al.*, Full electrical manipulation of perpendicular exchange bias in ultrathin antiferromagnetic film with epitaxial strain, Nat. Commun. **15**, 4734 (2024).

[56] S. Jiang, J. Shan, and K. F. Mak, Electric-field switching of two-dimensional van der Waals magnets, Nat. Mater. **17**, 406 (2018).